CORRELATION BETWEEN VELOCITY AND HEAT TRANSFER NEAR REATTACHMENT POINT BEHIND A BACKWARD FACING STEP

Shunsuke Yamada
Department of Mechanical Engineering
National Defense Academy
Hashirimizu, 1-10-20, Yokosuka, Kanagawa, 239-8686, Japan
yamadas@nda.ac.jp

Yuki Funami
Department of Mechanical Engineering
National Defense Academy
Hashirimizu, 1-10-20, Yokosuka, Kanagawa, 239-8686, Japan
funami@nda.ac.jp

Hajime Nakamura
Department of Mechanical Engineering
National Defense Academy
Hashirimizu, 1-10-20, Yokosuka, Kanagawa, 239-8686, Japan
nhajime@nda.ac.jp

ABSTRACT

In this study, the mechanism of heat transfer enhancement near the reattachment point behind a backward facing step is experimentally investigated at Reynolds number of 5400. The unsteady fluctuations of the velocity and temperature are simultaneously measured by using 2 dimensions and 3 components (2D-3C) Particle Image Velocimetry (PIV) and the high-speed infrared (IR) thermography. To discuss the temporal-spatio correlations of the velocity and the heat transfer fluctuations, 3 components of the velocity and the heat transfer coefficient are calculated from direct cross-correlation method and unsteady heat conduction equation. Also, these time history data are analysed by using continuous wavelet transform and two-point correlation. As a result, the flow behaviour induced by the streamwise vortex and heat transfer enhancement present a high correlation with the characteristics frequency.

INTRODUCTION

The insight of the heat transfer in the separated and reattachment flow is very important to develop the cooling technique for the electric devices, nuclear reactor, turbine blade and many heat transfer devices. Many researchers have investigated the aspects of fluid and thermal dynamics over a backward facing step as the simple model of the separated and reattachment flow. Recently, the detail review of this flow has been summarized by Chen et al., (2018). Many studies focus on the enhancement of the heat transfer, and the flow and thermal fluctuations downstream of a backward facing step, because there is the complicated flow that included the free shear layer by flow separation, vortex motion and reattachment flow. Vogel and Eaton, (1984) reported that the location of the maximum peak of the heat transfer has corresponded to that of root-mean square of the skin friction coefficient. Also, Avancha and Pletcher, (2002) indicated that the heat transfer has been relationship with the thickness of the viscous sublayer. On the other hand, the flow fluctuation near the reattachment point has the characteristics frequency of fu_0/H of about 0.2 and 0.06, at which the fluctuating motion of the vortex and the flapping in the shear layer appear near the reattachment point (Driver et al., 1987, Le et al., 1997 and Lee and Sung, 2001). However, there are little reports about the thermal fluctuation, and it is not enough to clarify the periodic phenomenon of the flow and thermal fields.

In order to understand the temporal-spatio periodicity of the flow and thermal behaviour, it is required to measure with the high temporal-spatio resolutions. We suggested the simultaneous measurement of the flow and the thermal field using 2D-3C PIV and a high-speed infrared (IR) thermography combined system (Yamada and Nakamura, 2016). The correlation of each velocity in the *xz* cross section and heat transfer coefficient on the heated wall were investigated behind a backward facing step.

In this paper, the temporal-spatio fluctuations of the velocity in *yz* cross section under the step and temperature on the heated wall is investigated near the reattachment point at Re_H of 5400. Also, the temporal-spatio correlated relationship between the velocity and heat transfer coefficient is analysed by using continuous wavelet transform and two-point correlation.

EXPERIMENTAL SETUP AND METHOD

Wind tunnel and co-ordinate system

The experiments were carried out in a blower-type wind tunnel having a rectangular cross section of 400 mm in height and 150 mm in width. Figure 1(a) shows the test section, and the present experiments was conducted by turning it upside down considering buoyancy effect. A flat plate of 900 mm in length was located so that the channel height upstream of a backward facing step was 100 mm. The turbulent boundary layer was created by a tripping wire of 2 mm in diameter at downstream of 20 mm from the edge of a flat plate. The step height, H, was 20 mm. The expansion ratio, *ER* was 1.2, and the aspect ratio in the spanwise direction based on this step height 7.5. The bottom wall of the step side behind the step edge was heated for heat transfer measurement.

The origin of the coordinate system is at mid-span of the bottom wall of the step edge in Fig. 1(b). In this coordinate system, the flow velocity in the streamwise, transverse and spanwise directions (*x*, *y* and *z*) corresponds to *u*, *v*, *w*, respectively. The main stream velocity, u_0, is fixed at 4 m/s upstream of this step. The streamwise turbulent intensity of

the mainstream is approximately 0.5 %. Reynolds number, Re_H, based on the step height and the mainstream velocity is at about 5400.

Figure 1(b) shows a schematic diagram of the heated plate. The heated plate was fabricated from acrylic resin and had 7 sections removed. These sections were covered with the thin titanium foil sheets (61 mm in length, 100 mm in width, and 2.1 μm in thickness) arranged in the streamwise direction. In the heated plate, air layers of 1 mm in thickness exist between the heated titanium foil and the aluminium plate (see Fig. 1(b)). Since the titanium foil and the aluminium plate are heated to the almost same temperature, the heat conduction loss inside the test plate is suppressed. The temperature inside the heated aluminium plate was measured by thermocouples (T C) at x = 62.5, 124.5, 186.5, 248.5, 310.5 and 372.5 mm. Both sides of these thin foils were tightly adhered to electrodes with a high-conductivity bond in order to suppress contact resistance. 7 sheets of these foils were heated by direct current at the constant heat flux of approximately 410 W/mm^2. The titanium foil sheets are stretched in response to tension, because the thermal expansion coefficient of the heated acrylic resin is greater than that of the titanium foil. The temperature of the heated foil was measured using a high-speed IR thermograph, so that high-speed thermal fluctuation has been observed due to the low heat capacity of these thin foils.

Experimental apparatus of 2D-3C PIV and High-speed IR thermograph

In Fig. 1(c), the shutters of 2 cameras (Motion Scope M3, IDT), IR thermograph (SC4000, FLIR), and the emission of Nd: YAG laser (HFYA-10SD, SEIKA Digital Image Corp.) are synchronized by the timing controller. As shown in Fig. 1(d), the high-speed cameras and the IR thermograph were arranged. The camera frame rates for PIV and the IR thermography, were at 1000 frames per second (fps). The physical sizes of the velocity and the temperature images are in the range of z/H from -1.5 to 1.5 under the step at x/H = 4.5 mm near the reattachment point, and x/H from 3.1 to 6.0 and z/H from -1.5 to 1.5 on the heated wall. The heat transfer coefficient was calculated from unsteady heat conduction equation using the time history data of temperature distributions.

2D-3C PIV system

The 2D-3C PIV system consisted of a Nd: YAG laser with light-sheet optics and 2 CMOS cameras of resolution 512 × 256. Air flow was seeded with the DOS (dioctyl sebacate) particle of an average diameter of about 1 μm. The seeding density was about 10 particles per interrogation area in the laser light sheet of about 1mm in the thickness and the size of the interrogation was 16 × 16 pixels with 50 % overlap. The time intervals between the pair images were set to 50 μs at the main stream velocity u_0 = 4 m/s, and 4000 pair images were captured by 2 cameras arranged in stereo. 3 velocity components were calculated from the direct-cross correlation method and the camera function by using commercial software (ProVISION-XS ver. 3.13, IDT)

Calculation procedure of convective heat transfer

The temperature distributions, T_w on the heated wall photographed by IR Thermograph was obtained from the following equation:

$$\boldsymbol{E = \varepsilon f(T_w) + (1-\varepsilon) f(T_{amb})} \quad (1)$$

where E is the spectral emissive power detected by IR thermograph, f(T) is the calibrated function of the IR thermograph as the black body, and ε is the spectral emissivity of this foil for IR thermograph. The terms on the right-hand

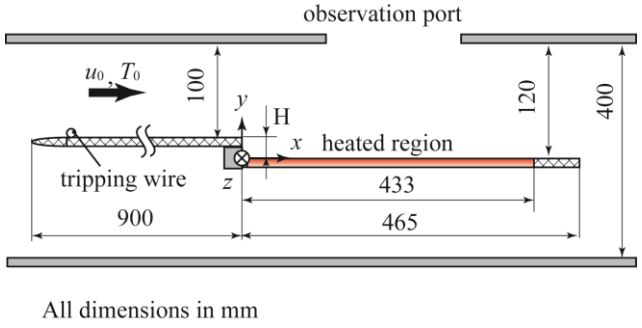

(a) Wind tunnel

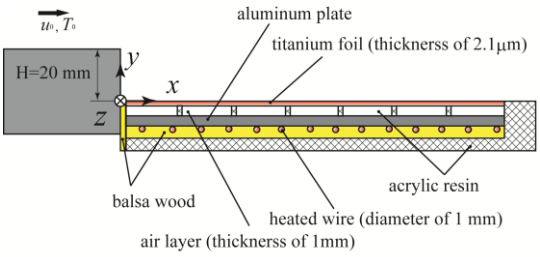

(b) Heated plate

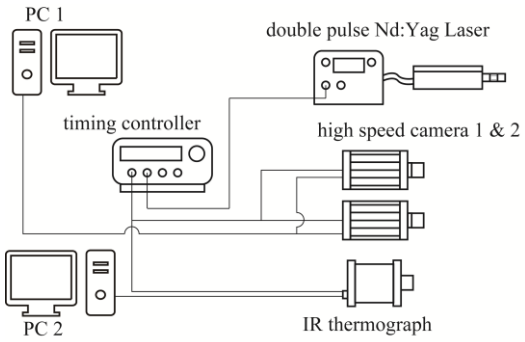

(c) Simultaneous measurement system

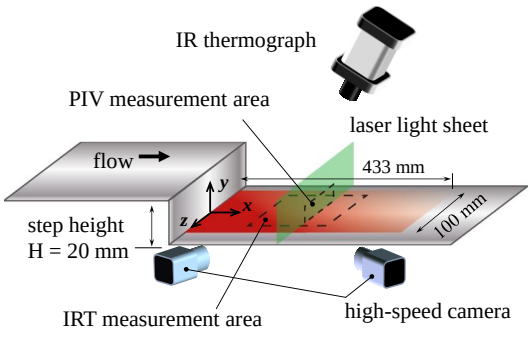

(d) Camera arrangement of PIV and IR thermography

Figure 1 Schematic diagram of experimental apparatus.

side of Eq. (1) denote the emissive powers at the temperature of the heated wall, T_w, and the ambience, T_{amb}, respectively. In this measurement, the distance between IR thermograph and the heated wall was approximately 400 mm, so that the transmittance of the air was approximately 1.0.

Figure 2 shows a schematic diagram of the heat transfer model from the heated plate. The local and instantaneous heat transfer coefficients are obtained from the following equations that translated unsteady heat conduction equation:

$$\boldsymbol{h = \frac{\dot{q}_{in} - \dot{q}_{cd} - \dot{q}_{rd} - \dot{q}_{rdi} + A - B}{T_w - T_0}} \tag{2}$$

Where

$$\boldsymbol{A = \lambda_t \delta_t \left(\frac{\partial^2 T_w}{\partial x^2} + \frac{\partial^2 T_w}{\partial z^2} \right)} \tag{3}$$

and

$$\boldsymbol{B = c_t \rho_t \delta_t \left(\frac{\partial T_w}{\partial t} \right)} \tag{4}$$

where c_t, ρ_t, λ_t and δ_t are specific heat, density, thermal conductivity and the thickness of the titanium foil, respectively. And $\dot{q}_{in}$ is the input heat fluxes to the foils due to the Joule heating, $\dot{q}_{cd}$ is the heat fluxes from the foil due to the conduction, and $\dot{q}_{rd}$ and $\dot{q}_{rdi}$ are the radiation heat fluxes out of and into the heated plate, respectively. The translated heat conduction equation, given by Eq. (2), includes both lateral heat conduction through the foil given by Eq. (3) and the temporal delay due to the heat capacity of the foil given by Eq. (4). The heat conduction to the air layer inside the heated plate is calculated based on the temperature distribution inside the air layer (thickness δ_a = 1 mm in Fig. 2), which can be determined by solving the following heat conduction equation of Eq. (5).

$$\boldsymbol{\dot{q}_{cd} = -\lambda_a \left(\frac{\partial T_a}{\partial y} \right)\Big|_{y=0}} \tag{5}$$

and

$$\boldsymbol{c_a \rho_a \frac{\partial T_a}{\partial t} = \lambda_a \left(\frac{\partial^2 T_a}{\partial x^2} + \frac{\partial^2 T_a}{\partial y^2} + \frac{\partial^2 T_a}{\partial z^2} \right)} \tag{6}$$

where c_a, ρ_a and λ_a are specific heat, density and thermal conductivity of the air. The temperature of the aluminium plate measured by the thermocouples (TC) is the boundary condition for calculating the temperature of the air layer from Eq. (6). The temperature of the air layer inside the heated plate, T_a, is calculated using the alternative direction implicit (ADI) method with respect to the x and z directions.

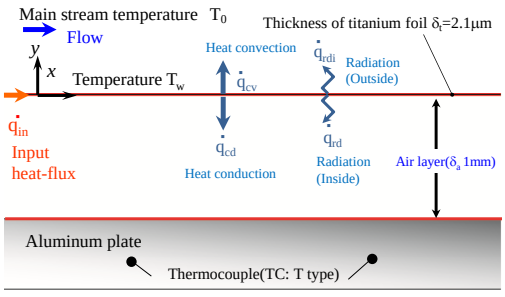

Figure 2. Model of the heat transfer in the heated plate.

The finite difference method was used to calculate the heat transfer coefficient, h, using Eq. (2). The discretization of the spatial derivative terms of Eq. (3) and the temporal derivative term of Eq. (4) applied to the second-order central difference with the mean pixel spacing ($\Delta x \approx 0.43$, $\Delta z \approx 0.56$ mm) and the central difference with the time step of a frame interval (the frame rate of IRT is 1000 fps; Δt = 1 ms). A low-pass filter was set to the temporal and spatial directions (cut-off frequency f_{cut} and wavenumber k_{cut} under 123 Hz and 0.29 mm^{-1}), respectively (Nakamura and Yamada, 2013).

Comparison of experimental and numerical data

Figures 3 show the time-averaged velocity profiles in the streamwise (a) and transverse (b) directions in yz cross section at x/H and z/H of about 4.5(near the reattachment point) and 0. For comparison, these figures include the DNS data of Le et al (1997) at Re_H = 5100 and x/H of 6.0. The present reattachment length is shorter than the typically 2 dimensional cases in the same Reynolds number. The present and DNS mean velocities indicate similar tendency, however the difference between the present and DNS data increase away from the wall in Fig. 3(a) and (b). In the case of the low aspect ratio, the vorticity induced by the shear layer spreads toward the wall and increases the spanwise entrainment and downwash flow near the center of the step (Shin and Ho, 1994). Therefore, the reattachment length is shorter than that, and the velocity profile does not agree with both.

Figure 4 shows the time-averaged local Nusselt number at Re_H = 5400, and LES data of Avacha and Pletcher (2002) at Re_H = 5540. Both profiles present the similar tendency, however the difference of the maximum value is about 5.4 %. This is caused by the difference of the shear layer associated with the expansion and aspect ratios.

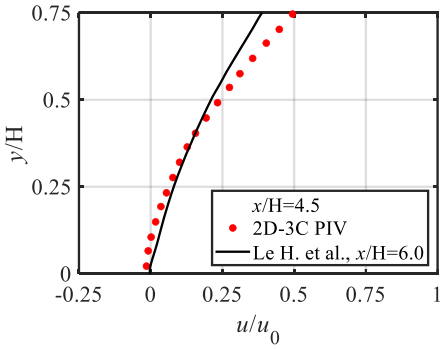

(a) Streamwise direciton

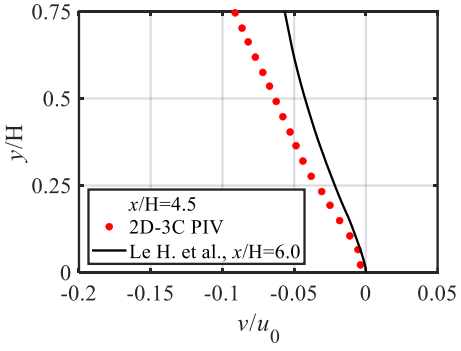

(b) Transverse direction

Figure 3. The time-averaged velocity profiles near the reattachment point.

EXPERIMENTAL RESULTS AND DISCUSSIONS

Instantaneous distribution and wavelet analysis

Figure 5 shows the instantaneous velocity vectors, *v*, *w* and contour map *u* (top), and heat transfer coefficient profile, *h* (bottom) at *x*/H of 4.5. In Fig. 5, the instantons flow field near the reattachment point occurs complicated state and the heat transfer has the spatial-periodic fluctuation. Also, the local downwash flow is formed by the streamwise vortex.

Wavelet analysis applied to the backward facing step flow (Lee and Sung, 2001). Continuous wavelet transform was used for the time history data of the velocities and heat transfer coefficient, and it is possible to reveal the existence of short-lived and quasi-periodic events. Figures 6 show the time history of velocities and wavelet coefficient in the streamwise (a) and transverse (b) direction, and heat transfer coefficient (c), respectively. In these figures of the contour map of wavelet coefficient, these vertical axes indicate the logarithm. Morlet wavelet function was used in the present analysis. The peak of wavelet coefficients of velocity and heat transfer appear in non-dimensional frequency range from about 0.06 to 0.20. In the free shear layer, the frequency appears at $f \cdot \mathrm{H}/u_0$ of about 0.2 due to the large vortex structure. In addition to this frequency, there is the peak at the low frequency, $f \cdot \mathrm{H}/u_0$ of about 0.06. The low frequency is possibly due to the appearance of the flapping motion (Driver et al, 1987). In this study, it seems that the low frequency near about 0.06 corresponds to the downwash flow induced by the flapping motion.

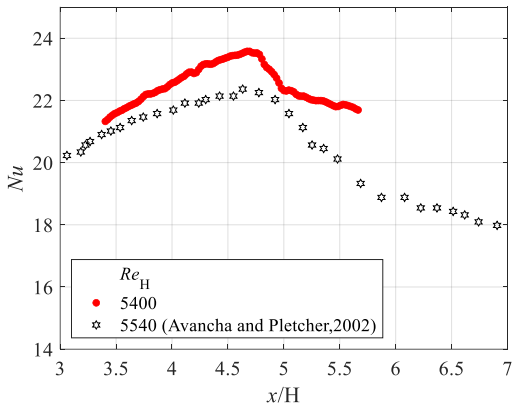

Figure 4. Time-averaged local Nuselt number

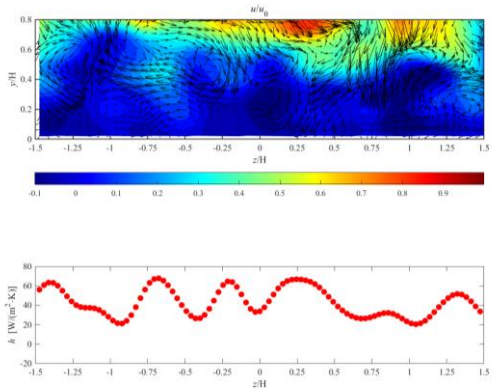

Figure 5. Instantaneous velocity (topside) and heat transfer coefficient (bottom) at $\mathrm{Re_H}$ of 5400.

Momentum and thermal transport induced by vorticities

The heat transfer fluctuation is relationship to the momentum transport due to the downwash flow induced by the streamwise vortex. To detect the vortex in *yz* cross sectional flow, the vorticity, Ω_{yz} and the shear stress S_{yz} were calculated from Eq. (7) and (8). The strengths, Q_{yz} of the rotation and the shear stress were compered from Eq. (9), and

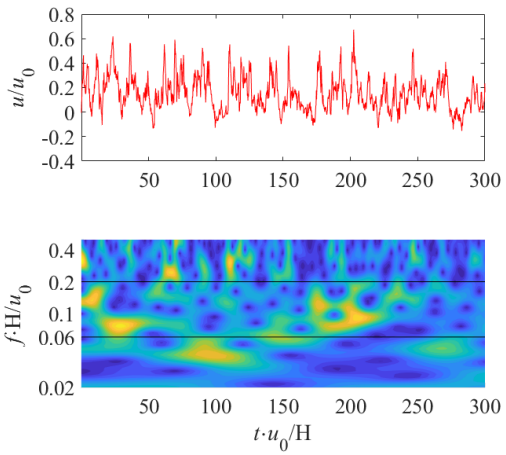

(a) Velocity in the streamwise direciton

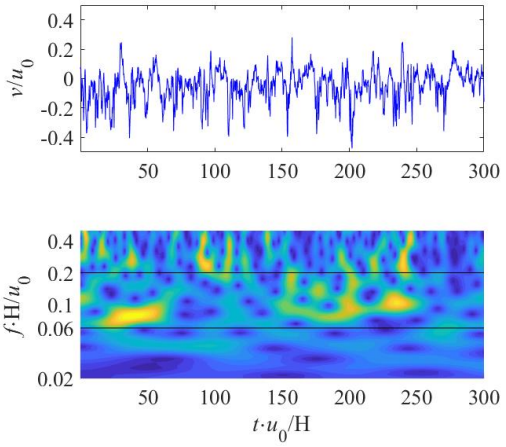

(b) Velocity in the transverse direciton

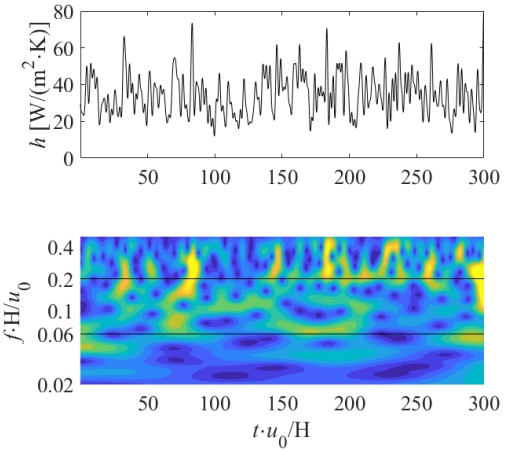

(c) Heat trasfer coefficinet

Figure 6. Time history data (top) and wavelet coefficient (bottom) of each velocity and heat transfer coefficient at $\mathrm{Re_H}$ of 5400, and z/H and *y*/H of 0.0 and 0.41.

the zone above a certain threshold, Q_{th} was defined as the vortex region, Q_{vortex} in Eq. (10)

$$\boldsymbol{\Omega_{yz}(y,z,t)} = \frac{1}{2}\left(\frac{\partial w}{\partial y} - \frac{\partial v}{\partial z}\right) \tag{7}$$

$$\boldsymbol{S_{yz}(y,z,t)} = \frac{1}{2}\left(\frac{\partial w}{\partial y} + \frac{\partial v}{\partial z}\right) \tag{8}$$

$$\boldsymbol{Q_{yz}(y,z,t)} = \frac{1}{2}\left(-|S_{yz}|^2 + |\Omega_{yz}|^2\right) \tag{9}$$

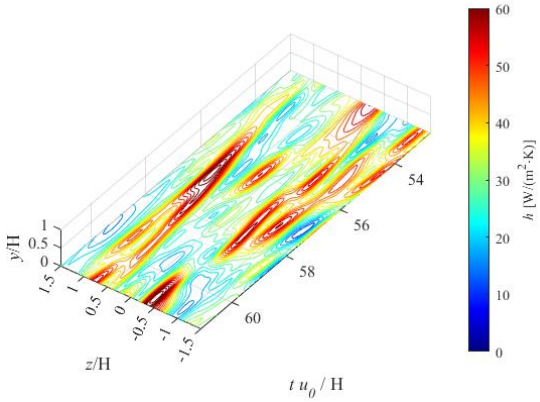

(a) Heat trensferr on the heated wall

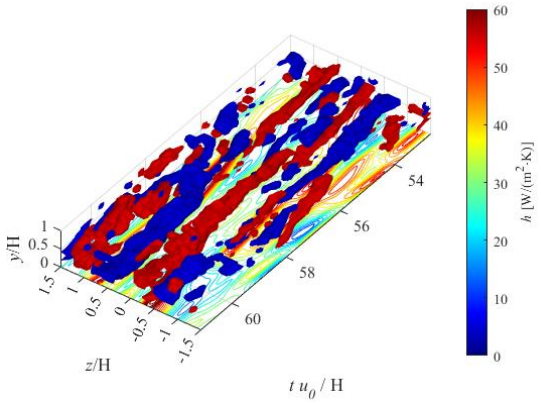

(b) Volticity in the yz cross section and heat treansfer

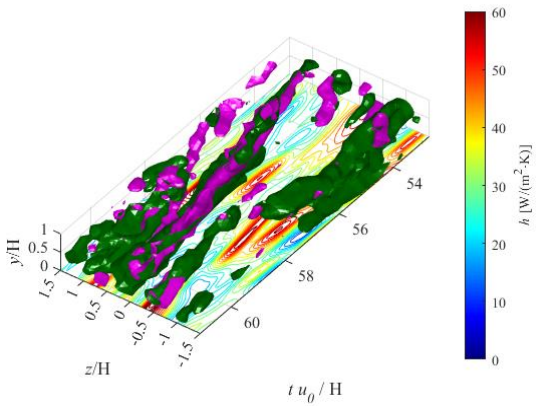

(c) Reynolds stress in the yz cross section and heat treansfer
Figure 7. The instataneous of the vortex structure and thermla flucutation.

$$\mathbf{Q}_{vortex}(y,z,t) = \begin{cases} \mathbf{1} & if\ Q_{yz} > Q_{th} \\ \mathbf{0} & otherwise \end{cases} \tag{10}$$

From reult of Q_{vortex}, it is possible to creat the isosurface of vortcity in the *yz* cross section. In this study, a certain threshold, Q_{th} was more than 8000 [1/s^2]. Also, the region of the high mometum trasport was detected from Reynolds stress, *uv* and *uw*. Similar to determination of this vortex region, the isosurface of the mometum trasport was created from these thresholds of Reynolds stress less than *uv* of 0 m^2/s^2 and more than $(uw)^2$ of 0.02 m^4/s^4.

Figures 7 show the contour map of the time history of the heat trasfer coefficient at *x*/H of 4.5 (a), the isosurface of the vortex rigion (b) and the negative and high Reynolds stress region, *uv* and *uw* (c), respectively. In Fig. 7(b) and (c), the red and blue isosurfaces indicate the counter-crokweise and the crockwise of the rotation, and the green and magenta isosurfaces the negative and the high regions of the Reynolds stress, *uv* and *uw*. As shown in Fig. 7(a), the thermal spot and thermal streaks apper on the heated wall. In Fig. 7(b), as well as heat trasfer coefficient, the vorticies have the streakly structure toward the time, and are arranged periodically in the spanwise direction. Figure 7(c) shows that the negative and high Reynolds stress regions, *uv*, *uw* apper near the thremal spots and streaks.

Two-point correlation of flow and thermal fluctuations

To investigate flow and thermal structure quantitatively, a two-point correlation coefficient, R_{nn} was calculated from Eq. (11).

$$\boldsymbol{R_{nn}(y,\Delta z,\Delta t)} = \frac{\boldsymbol{n'(y,z,t) - n'(y,z+\Delta z,t+\Delta t)}}{\sqrt{\boldsymbol{n'^2(y,z,t)}}\sqrt{\boldsymbol{n'^2(y,z+\Delta z,t+\Delta t)}}} \tag{11}$$

where the fluctuations of each velocity and heat transfer coefficient are substituted for *n´*. Also, these analysis data were used in the non-dimensional time range $t \cdot u_0/H$ from about 160 to 180 when the peak of the wavelet coefficient appeared in Fig. 6. Contour map of two-point correlation coefficient of heat transfer coefficient is shown in Fig. 8. Figures 9 shows the contour map of two-point correlation coefficient of each velocity at *y*/H of 0.4(a) and 0.8(b). In Fig. 8, the high peak value of the correlation coefficient is confirmed at the origin, and there are the weak peaks at Δz/H of about -1.0 and 1.0, and Δ*t* u_0/H of 0.0. Figures 9(a) present that, as same as the heat transfer correlation, the fluctuating correlations of the streamwise, transverse and spanwise velocities appear at Δz/H of about -1.0, 0 and1.0, and the correlation peak of the streamwise and transverse velocity fluctuations are stretched toward the non-dimensional time. Also, these peaks of the transverse velocity fluctuations have more clearly and higher than that of the streamwise and spanwise velocity fluctuations. However, in Fig. 9(b), these special peaks of the velocity fluctuations become weak less than that of the velocity fluctuations in Fig. 9(a). As a result, the special correlation of the heat transfer corresponds to the velocity fluctuation at *y*/H of 0.4, and the non-dimensional correlation lengths Δz/H is about 1.0. Keating et al., (2004) reported that the thermal spot corresponds to the intermittent downwash flow near the reattachment region.

SUMMARY

In this study, the velocities in *yz* cross section near the reattachment point and the temperature on the heated wall were simultaneously measured by 2D-3C PIV and IR thermography at Re_H of 5400. The time history of the streamwise vortex and the heat transfer coefficient were calculated from the velocity and temperature profiles. Using continuous wavelet transform and two-point correlation, the characteristic frequency and the temporal-spatio correlations of the velocity and heat transfer were investigated. Consequently, the frequency peaks of the velocity and the heat transfer coefficient appear in the non-dimensional periodic range from 0.06 to 0.2, and the spatial correlation length in the spanwise direction are at Δz/H of about 1.0, when the high wavelet coefficients appear at *y*/H of 0.4.

REFERENCES

Avancha, V. R. R., and Pletcher, H, R., 2002, "Large eddy simulation of the turbulent flow past a backward-facing step with heat transfer and property variance", *Int. J. Heat and Fluid Flow*, Vol. 23, pp. 601-614.

Chen, L., et al., 2018, "A review of backward-facing step (BFS) flow mechanisms, heat transfer and control", *Therm. Sci. Eng. Prog.*, Vol. 6, pp. 194-216.

Driver, M. D., Lee Seegmiller H., and Marvin, G. J., 1987, "Time-dependent behaviour of a reattaching shear layer", *AIAA J.*, Vol. 25, No. 7, pp. 914-6919.

Keating, A., Piomelli, U., Bremhorst, K., and Nešić, S., 2004, "Large-eddy simulation of heat transfer downstream of a backward-facing step", *J. Turbulence*, Vol. 5, N20.

Le, H., Moin, P., and Kim, J., 1997, "Direct numerical simulation of turbulent flow over a backward-facing step", *J. Fluid Mech.*, Vol. 330, pp. 349-374.

Lee, I., and Sung, J., 2001, "Characteristics of wall pressure fluctuations in separated flows over a backward-facing step: Part II: Unsteady wavelet analysis", *Exp. Fluids*, Vol. 30, pp. 273-282.

Nakamura, H., and Yamada, S., 2013, "Quantitative evaluation of spatio-temporal heat transfer to a turbulent air flow using a heated thin-foil", *Int. J. Heat Mass Transf.*, Vol. 64, pp. 892-902.

Shin, C., and Ho, C-H., 1994, "Three-dimensional recirculation flow in a backward facing step", *J. Fluids Eng.*, Vol. 116, pp. 228-232.

Vogel, J. C., and Eaton, J. K., 1985, "Combine heat transfer and fluid dynamic measurements downstream of a backward facing step", *J. Heat Transfer*, Vol. 107, pp. 922-929.

Yamada, S., and Nakamura, H., 2016, " Construction of 2D-3C PIV and high-speed infrared thermography combined system for simultaneous measurement of flow and thermal fluctuations over a backward facing step ", *Int. J. Heat Fluid Flow*, Vol. 61, pp. 174-182.

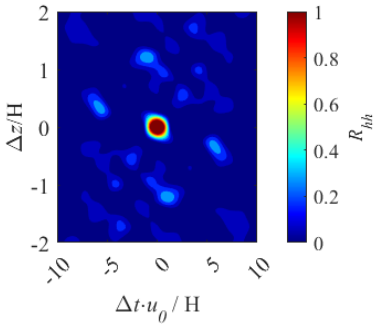

Figure 8. Contour map of the two-point correlation of *h*.

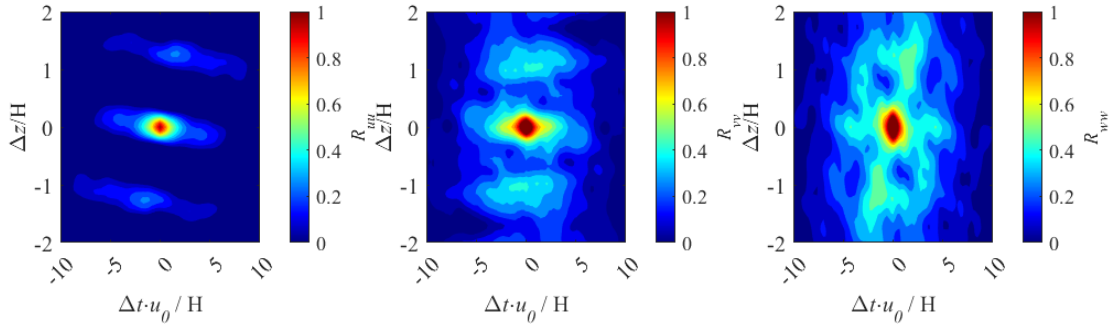

(a) Corrrelation coeffieint at *y*/H = 0.4(left: *u´*, cener: *v´*, rigtht: *w´*)

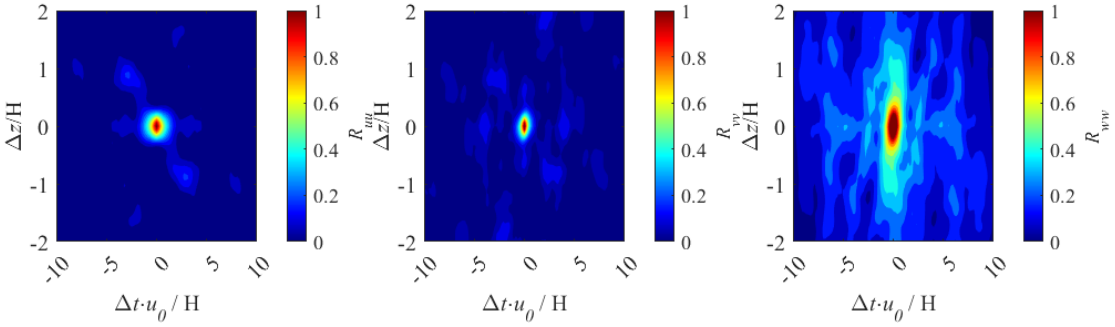

(b) Corrrelation coeffieint at *y*/H = 0.8 (left: *u´*, cener: *v´*, rigtht: *w´*)

Figure 9. Contour map of two-point correaltion of velocity fluctuations.